Journal of Engineering and Sustainable Development
المجلد 22، العدد2 (الجزء-2)، آذار2018
ISSN 2520-0917
10.31272/jeasd.2018.2.22

INVESTIGATION OF THE EFFECT OF DUCT HEIGHT ON THE PERFORMANCE OF SOLAR AIR HEATER WITH BAFFLES

*Dr. Jalal Mohammed Jalil[1], Dr. Ghaidaa Kaain Salih[2], Yousif Ali Madhi

1) Prof., Electromechanical Engineering Department, University of Technology, Baghdad, Iraq.
2) Prof., Asst., Electromechanical Engineering Department, University of Technology, Baghdad, Iraq.
3) M.Sc., Electromechanical Engineering Department, University of Technology, Baghdad, Iraq.

Abstract: In this study, solar air heater with straight shaped baffles is investigated numerically and experimentally to improve the thermohydraulic performance by changing the height of the duct to find the optimum value. Numerically, steady state 3D forced convection turbulent model is used to solve Navier Stokes and energy equations of airflow inside rectangular duct of solar air heater. The results showed that, the 3.75 cm duct height with air mass flow rate of 0.05 kg/s yields the highest effective efficiency. In addition, the results showed that the 2.5 cm duct height gives the highest effective efficiency for mass flow rate up to 0.0375 kg/s and it decreases as mass flow rate increases due to excessive differential pressure developed across the duct.

Keywords: *CFD, Solar air heater, Effective efficiency*

تحقيق في تأثير ارتفاع قناة هوائية على اداء مسخن هوائي شمسي مع حواجز

الخلاصة: في هذه الدراسة تم بحث مسخن حراري شمسي مجهز بحواجز مستقيمة الشكل عدديا وتجريبيا لتحسين الأداء الحراري والهيدروليكي عن طريق تغيير ارتفاع القناة الهوائية لايجاد انسب قيمة. عدديا، استخدم نموذج لحالة مستقرة ثلاثية الابعاد ذات تيارات حمل قسرية مضطربة لحل معادلات نافير ستوكس ومعادلة الطاقة لتدفق الهواء داخل قناة مستطيلة الشكل من سخان الهواء بالطاقة الشمسية. اظهرت النتائج ان قيمة الارتفاع 3.75 سم مع تدفق هوائي بمقدار 0.05كغم/ثا يعطي افضل كفائه مؤثرة. بالاضافه الى ذلك اضهرت النتائج ان الارتفاع 2.5 سم يعطي افضل كفاءة مؤثرة لتدفق هوائي حتى 0.0375 كغم/ثا ثم تقل قيمة الكفاءة مع زيادة التدفق الهوائي بسبب فرق الضغط المفرط المتولد على طرفي القناة الهوائية.

1. Introduction

Solar air heater is simple thermal system used for low temperature heating. A transparent material sheet such as plastic or glass is fixed above the absorber plate and the system is insulated thermally from the back and from the sides [1]. The solar air heater is widely used for domestic space heating and crop drying (grains, fruit, vegetables, etc.). The main disadvantage is low thermal efficiency because of low heat capacity and low thermal conductivity of the air. To make a solar air heater more effective solar energy utilization system, heat has to be transferred efficiently from the absorber to the flowing air. This will decrease absorber plate temperature and thus

*jalalmjalil@gmail.com

minimize convection and radiation losses through the glass. With improvements in design and manufacturing materials which lead to higher efficiency and low cost, solar air heaters can find new application in industry such us (1) Air pre-heating for combustion processes. (2) Drying minerals, coal, paper. (3) Space heating for warehouses, factories.

The performance of solar air heater was studied widely in recent years. Several technicalities were used to estimate the thermo-hydraulic performance of solar air heater. Karwa et al. [2] investigated the performance of solar air heaters with chamfered rib-roughness on the absorber plates. Aharwal et al. [3] examine a rectangular duct roughened with square rib split with a gap arranged at an inclination with direction of flow. Lanjewar et al. [4] studied experimentally W shaped ribs on absorber plate with two arrangements downstream and upstream to the flow.

Pottler et al. [5] stated that offset strip fins do not show an improved performance when compared to optimally spaced continuous fins, due to the fan power losses for this geometry. Priyam and Chand [6] evaluated analytically the performance of solar air heater with two transverse wavy fins. Falih [7] found that the inclined baffles with baffle pitch to duct height ratio of 1 gives higher heat transfer rate than the one with ratio of 2 and the smooth duct respectively, and the highest heat transfer and pressure drop is found by using baffle with 30°. Chamoli and Thakur [8] studied the performance of solar air heaters roughened with V down perforated baffles. Their Investigations have been performed using a mathematical model to study the effects of ambient conditions, operating and design on the effective efficiency.

Kumar et al. [9] deal with broken multiple V-type baffles. The results revealed that the broken multiple V-type baffles are thermo-hydraulically superior as compared to the other baffles. Kumar and Kim [10] showed that multi V-type perforated baffles performed better as compared to other shapes baffle in a rectangular duct. Karim and Hawlader [11], investigated flat plate, finned and V-corrugated solar air heaters. The V-corrugated collector was found to be the most efficient collector and the flat plate collector to be the least efficient.

In this work, solar air heater with straight shaped baffles is investigated numerically and experimentally to improve the thermohydraulic performance by changing the height of the duct to find the optimum value. The effective efficiency of solar air heater has been evaluated for three different values of duct height, which are 0.025, 0.0375 and 0.05 m, and four values of mass flow rate, which are 0.0125, 0.025, 0.0375 and 0.05 kg/s.

2. Mathematical Model

Numerically, steady state 3D forced convection turbulent hybrid scheme incompressible flow model is used to solve Navier Stokes and energy equations of airflow inside rectangular duct of solar air heater. The k-ε turbulence model is used for turbulent modelling.

I. Governing Equations

The governing equations are continuity, Navier Stokes and energy equations [12]:

$$\frac{\partial U}{\partial x}+\frac{\partial V}{\partial y}+\frac{\partial W}{\partial z}=0 \quad \dots (1)$$

$$\frac{\partial U^2}{\partial x}+\frac{\partial UV}{\partial y}+\frac{\partial UW}{\partial z}=-\frac{1}{\rho}\frac{\partial P}{\partial x}+\frac{\partial}{\partial x}\left(\nu_e\frac{\partial U}{\partial x}\right)+\frac{\partial}{\partial y}\left(\nu_e\frac{\partial U}{\partial y}\right)+\frac{\partial}{\partial z}\left(\nu_e\frac{\partial U}{\partial z}\right)+\frac{\partial}{\partial x}\left(\nu_e\frac{\partial U}{\partial x}\right)+\frac{\partial}{\partial y}\left(\nu_e\frac{\partial V}{\partial x}\right)+\frac{\partial}{\partial z}\left(\nu_e\frac{\partial W}{\partial x}\right) \quad \dots (2)$$

$$\frac{\partial UV}{\partial x}+\frac{\partial V^2}{\partial y}+\frac{\partial VW}{\partial z}=-\frac{1}{\rho}\frac{\partial P}{\partial y}+\frac{\partial}{\partial x}\left(\nu_e\frac{\partial V}{\partial x}\right)+\frac{\partial}{\partial y}\left(\nu_e\frac{\partial V}{\partial y}\right)+\frac{\partial}{\partial z}\left(\nu_e\frac{\partial V}{\partial z}\right)+\frac{\partial}{\partial x}\left(\nu_e\frac{\partial U}{\partial y}\right)+\frac{\partial}{\partial y}\left(\nu_e\frac{\partial V}{\partial y}\right)+\frac{\partial}{\partial z}\left(\nu_e\frac{\partial W}{\partial y}\right) \quad \dots (3)$$

$$\frac{\partial UW}{\partial x}+\frac{\partial VW}{\partial y}+\frac{\partial W^2}{\partial z}=-\frac{1}{\rho}\frac{\partial P}{\partial z}+\frac{\partial}{\partial x}\left(\nu_e\frac{\partial W}{\partial x}\right)+\frac{\partial}{\partial y}\left(\nu_e\frac{\partial W}{\partial y}\right)+\frac{\partial}{\partial z}\left(\nu_e\frac{\partial W}{\partial z}\right)+\frac{\partial}{\partial x}\left(\nu_e\frac{\partial U}{\partial z}\right)+\frac{\partial}{\partial y}\left(\nu_e\frac{\partial V}{\partial z}\right)+\frac{\partial}{\partial z}\left(\nu_e\frac{\partial W}{\partial z}\right) \quad \dots (4)$$

$$\frac{\partial UT}{\partial x}+\frac{\partial VT}{\partial y}+\frac{\partial WT}{\partial z}=\frac{\partial}{\partial x}\left(\Gamma_e\frac{\partial T}{\partial x}\right)+\frac{\partial}{\partial y}\left(\Gamma_e\frac{\partial T}{\partial y}\right)+\frac{\partial}{\partial z}\left(\Gamma_e\frac{\partial T}{\partial z}\right) \quad \dots (5)$$

To solve the governing Eqs. (1 to 5), mathematical expressions for effective kinematic viscosity, ν_e, and effective diffusion coefficient, Γ_e, are required through use of turbulence model. The standard *k*-ε model [13] has two equations, one for *k* and one for ε. It uses the following transport equations for *k* and ε.

$$\frac{\partial}{\partial x}(kU)+\frac{\partial}{\partial y}(kV)+\frac{\partial}{\partial z}(kW)=\frac{\partial}{\partial x}\left(\frac{\nu_t}{\sigma_k}\frac{\partial k}{\partial x}\right)+\frac{\partial}{\partial y}\left(\frac{\nu_t}{\sigma_k}\frac{\partial k}{\partial y}\right)+\frac{\partial}{\partial z}\left(\frac{\nu_t}{\sigma_k}\frac{\partial k}{\partial y}\right)+G-\varepsilon \quad \dots (6)$$

$$\frac{\partial}{\partial x}(\varepsilon U)+\frac{\partial}{\partial y}(\varepsilon V)+\frac{\partial}{\partial z}(\varepsilon W)=\frac{\partial}{\partial x}\left(\frac{\nu_t}{\sigma_\varepsilon}\frac{\partial k}{\partial x}\right)+\frac{\partial}{\partial y}\left(\frac{\nu_t}{\sigma_\varepsilon}\frac{\partial k}{\partial y}\right)+\frac{\partial}{\partial z}\left(\frac{\nu_t}{\sigma_\varepsilon}\frac{\partial k}{\partial z}\right)+C_{1\varepsilon}\frac{\varepsilon}{k}G-C_{2\varepsilon}\frac{\varepsilon^2}{k} \quad \dots (7)$$

$$G=\upsilon_t\left[2\left(\frac{\partial U}{\partial x}\right)^2+2\left(\frac{\partial V}{\partial y}\right)^2+2\left(\frac{\partial W}{\partial z}\right)^2+\left(\frac{\partial U}{\partial y}+\frac{\partial V}{\partial x}\right)^2+\left(\frac{\partial V}{\partial z}+\frac{\partial W}{\partial y}\right)^2+\left(\frac{\partial U}{\partial z}+\frac{\partial W}{\partial x}\right)^2\right] \quad \dots (8)$$

Where ε, is the dissipation term. The parametric values in this study are given in Table1.

Table 1 Empirical constants in the k-ε[13].

C_μ	$C_{1\varepsilon}$	$C_{2\varepsilon}$	σ_k	σ_ε
0.09	1.44	1.92	1.00	1.30

Numerical procedure called SIMPLE is used to solve the basic governing equations by using a hybrid scheme [14]. The finite volume mesh consists of many control volume using a staggered grid system. The simulations were conducted employing Fortran 90 language and the graphs were plotted using Tec plot. The accuracy of numerical solution is $5\text{x}10^{-3}$ for the present study that is reached at approximately $6\text{x}10^{3}$ iteration.

II. Boundary Conditions

The dimensions of the duct and baffles are shown in Fig. 1. Fig. 2 shows the schematic diagram and boundary conditions of the numerical model. The sides and bottom walls are insulated while the temperature of upper wall (absorber plate) is calculated by steady state three-dimension model. Energy balance method, which can be described as the summation of heat in and out equals to zero including solar term, are applied over small elements of six faces to calculate the temperature of absorber plate. The thermal radiation supplied to the solar air heater is fixed at 1000 W/m^2. The temperature of inlet air in the numerical solution is 25 C$^\circ$.

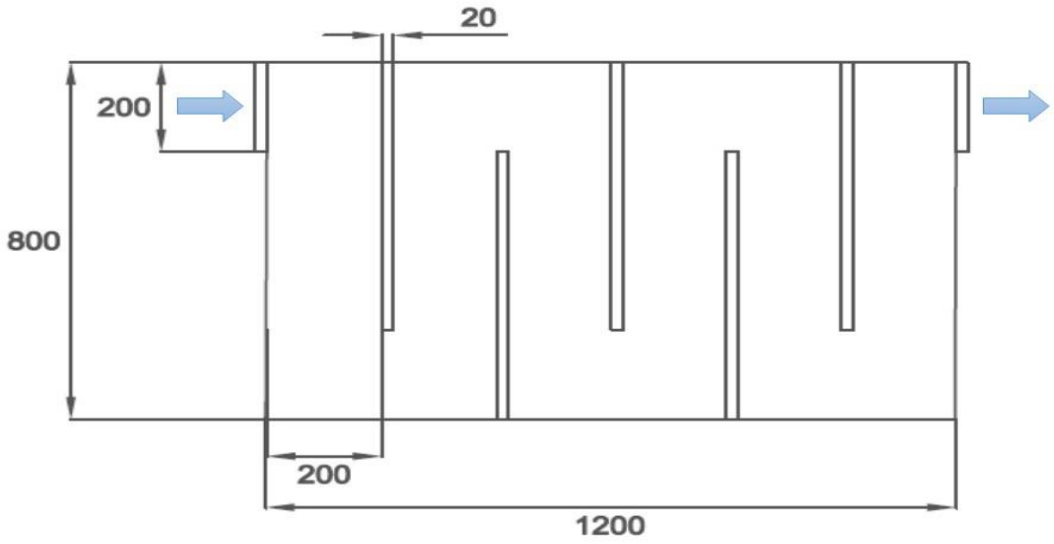

Fig. 1 Upper view of collector with dimensions for numerical and experimental models and directions of flowing air at inlet and outlet

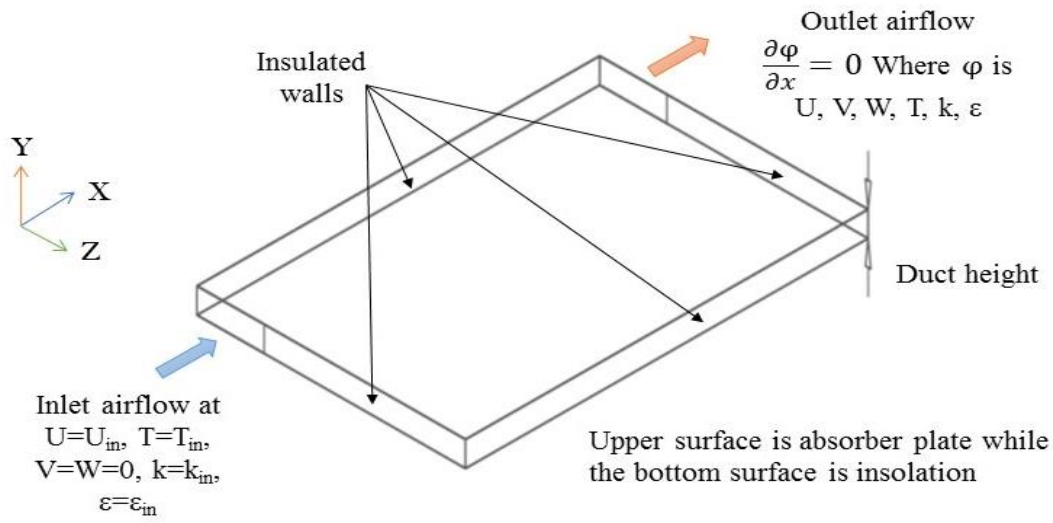

Fig. 2 Schematic diagram of numerical model with boundary conditions

III. Efficiency calculation

The useful power of solar air heater can be evaluated using [15]

$$Q_u = \dot{m}c_p(T_o - T_i) \quad \text{..... (9)}$$

Based on Eq. 10, the thermal efficiency of solar air heater can be calculated using

$$\eta_{th} = \frac{\dot{m}c_p(T_o - T_i)}{IA_c} \quad \text{..... (10)}$$

Thermohydraulic performance of solar air heater is evaluated on the basis of effective efficiency and is written as

$$\eta_{eff} = \frac{Q_u - P_m}{IA_c} \quad \text{..... (11)}$$

Where *Pm* is the mechanical energy required for air propelling through the duct which given by

$$p_m = \frac{\dot{m}\Delta p}{\rho} \quad \text{..... (12)}$$

3. Experimental Part

The experiment were conducted indoor to maintain the radiation intensity and air temperature.

So, bias results caused by different outdoor condition could be avoided. A schematic diagram of the experimental apparatus and cross section of the collector is shown in Fig. 3. The rectangular duct of plywood (represents the insolation of the sides and bottom) has an internal size of 1200*800*50 mm. A 1.5 mm-thick galvanised iron plate black matt painted is used as absorber plate and top wall of the duct. Full height baffles of galvanised iron welded on the lower surface of the absorber plate.

The air was the working medium and was supplied by 0.35 kW centrifugal fan. The flow rate was changed by controlling the inlet apertures of the fan. Four different values of mass flow rate which are 0.0125, 0.025, 0.0375 and 0.05 kg/s. The absorber plate is heated from the top by supplying radiative heat flux by means of sun simulator.

The absorber plate is covered by 4 mm thick normal window glass. Solar simulator is used with ten 500-W Tungsten Halogen lamps and solid-state voltage regulator. The value of irradiance is fixed on 1000 W/m^2. The thermal radiation received by the collector was measured using a Pyrometer placed on top of the cover glass. Fig. 4 shows digital photographs of the experimental apparatus.

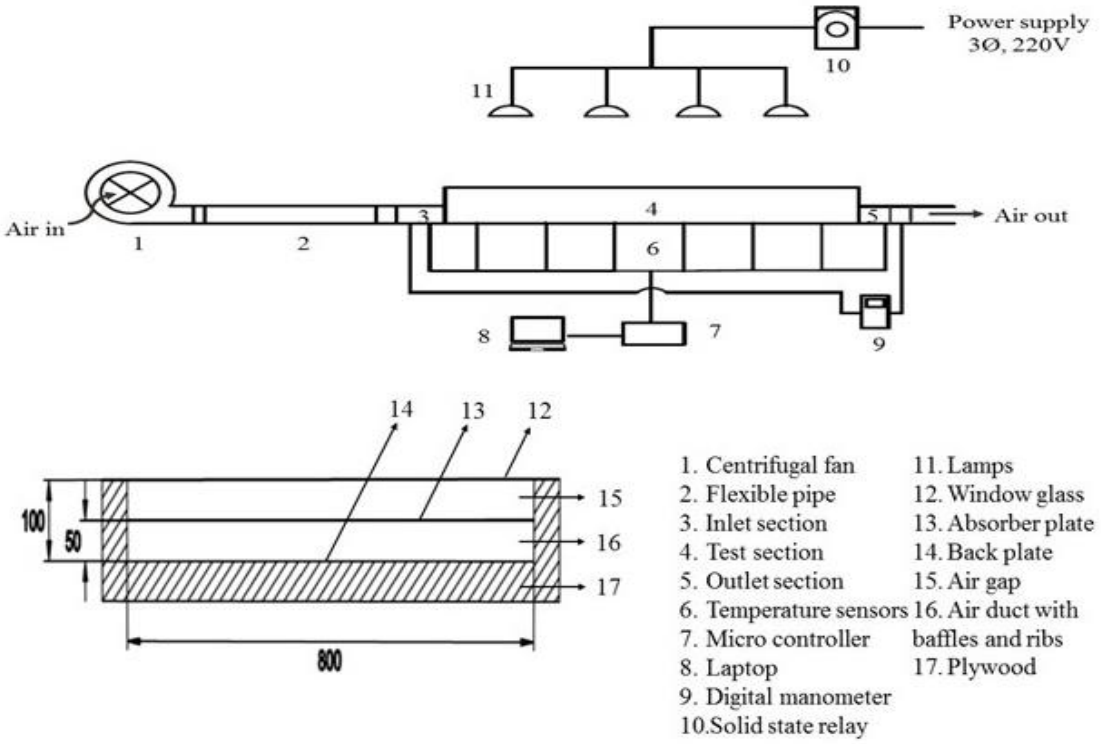

Fig. 3 Schematic drawing of the overall experimental system and cross section of the collector

Fig. 4 Digital photographs of the experimental apparatus

4. Validation of the code

The numerical model was in conditions similar to those of experimental arrangement. Fig. 5 compares between experimental and numerical variation of air

temperature difference across the duct with mass flow rate at fixed duct height of 5 cm. Figures seem good agreement is achieved between the experimental and numerical results. The deviation between experimental and numerical results have highest value of 1.3 C° and lowest value of 0.4 C°.

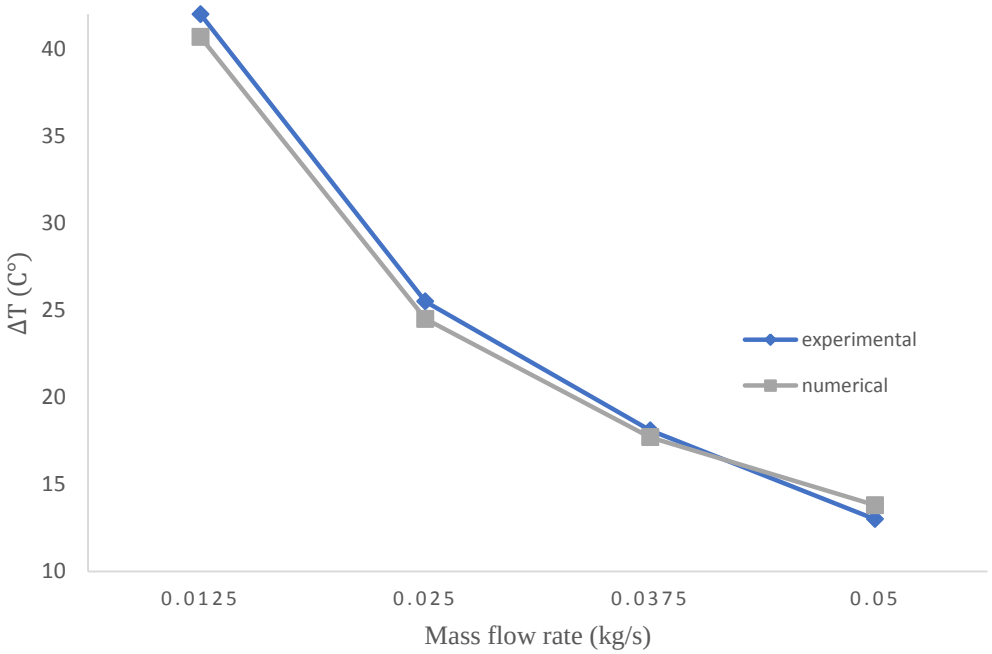

Fig. 5 Comparison between experimental and numerical variation of air temperature difference across the duct with mass flow rate.

5. Results and Discussion

Fig. 6 shows the Numerical variation of air temperature difference across the duct with mass flow rates for different values of duct height. From this figure, it is clear that the air temperature decrease rapidly as the airflow increases and reaches its lowest value at airflow of 0.05 kg/s. It can be seen that the air temperature decreases as the duct height increases and this reduction is high at low values of mass flow rate and becomes smaller at high values of mass flow rate.

Fig. 7 shows the Numerical variation of pressure difference across the duct with mass flow rates for different values of duct height. As shown in this figure the differential pressure across the duct at duct height of 2.5 cm is highly affected by the variation of mass flow rate compared with other values of duct heights. The differential pressure across the duct reaches its highest value of 700 pa at duct height of 2.5cm and mass flow rate of 0.05 kg/s.

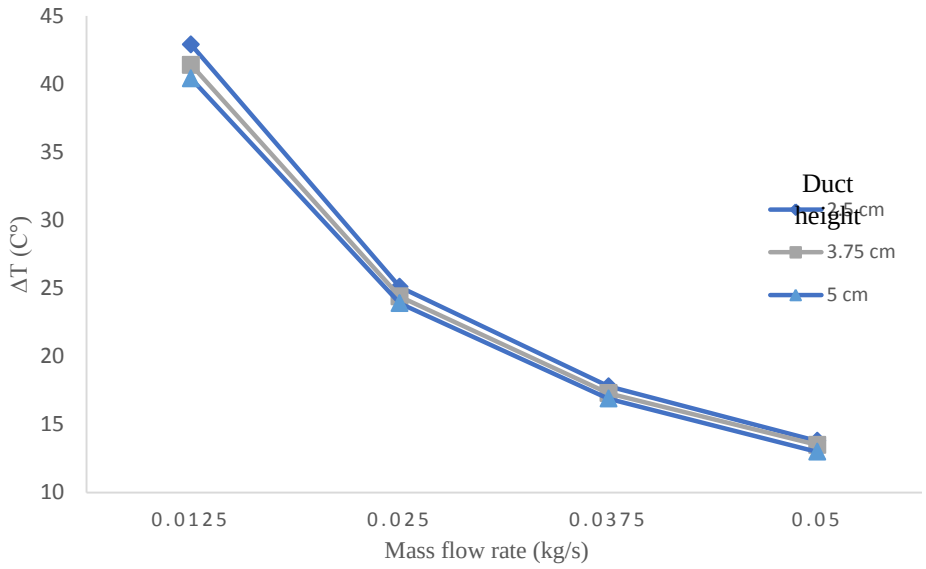

Fig. 6 Numerical Variation of air temperature difference across the duct with mass flow rates for different values of duct height

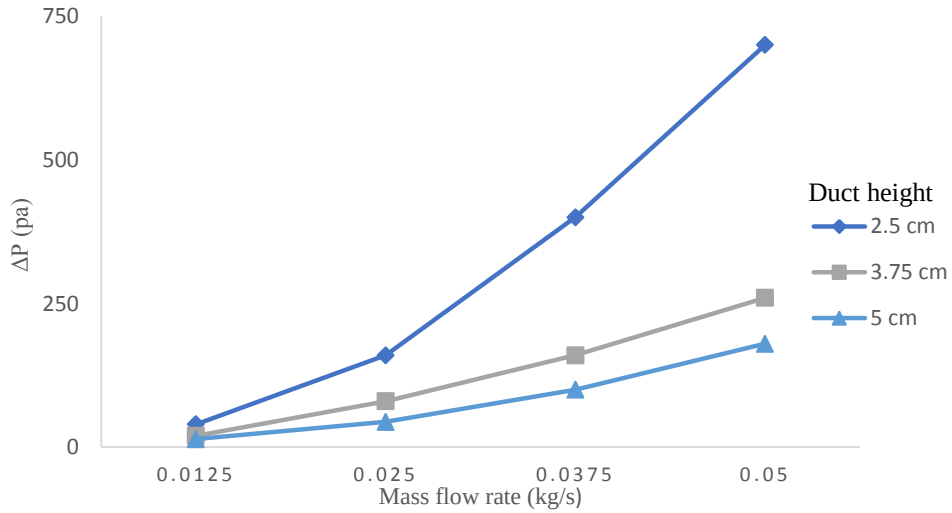

Fig. 7 Numerical Variation of air pressure difference across the duct with mass flow rates for different values of duct height

The variation of thermal efficiency of solar air heaters with mass flow rates for different values of duct height is shown in Fig. 8. Solar air heater with 2.5 cm has the highest thermal efficiency for the entire range of mass flow rates. The highest thermal efficiency obtained is 68.5% at mass flow rate of 0.05 kg/s and duct height of 2.5 cm.

The effect of hydraulic losses caused by reducing the duct height on the performance of solar air heater is shown in Fig. 9 in term of effective efficiency. The highest effective efficiency obtained for solar air heater is 65.5% at mass flow rate of 0.05 kg/s and duct height of 3.75 cm. In addition, the results showed that the effective efficiency of the solar air heater with 2.5 cm duct height has the highest value for mass flow rate up to 0.0375 kg/s and it decreases as mass flow rate increases due to excessive differential pressure developed across the duct.

Fig. 10 shows the velocity vectors for solar air heater with baffles at mass flow rates of 0.05 kg/s and duct height of 3.75 cm. It is clear from this figure the creation of boundary layer near the baffles. Fig. 11 shows the temperature contour (x z plane) at y = 2.7 cm for solar air heater with baffles at mass flow rate of 0.05 kg/s and duct height of 3.75 cm. The effect of straight baffles on air temperature as heat transfer surface can be seen clearly in the layers adjacent to the baffles.

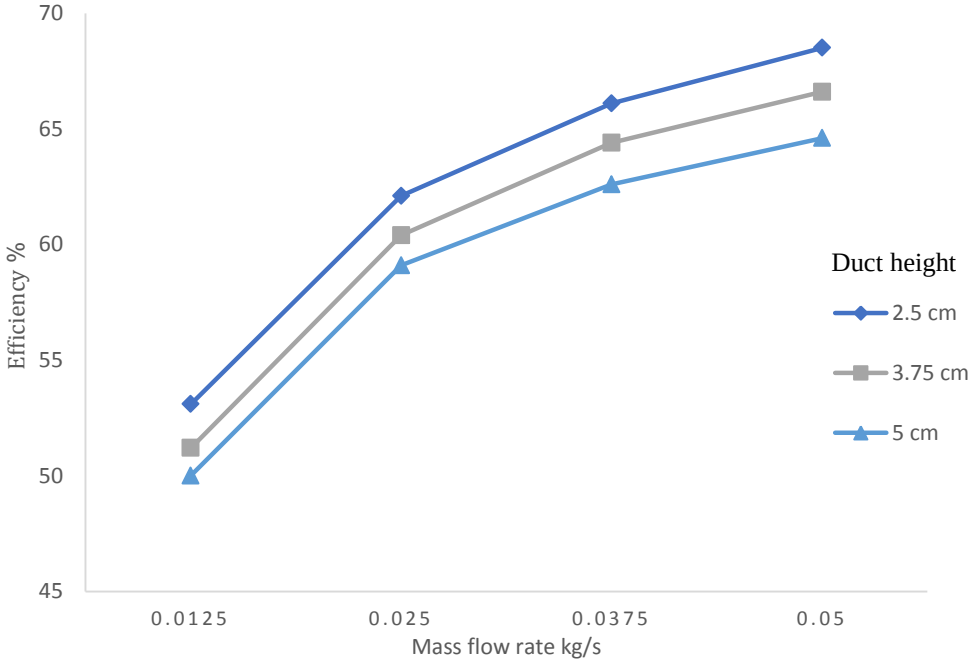

Fig. 8 Variation of thermal efficiency of solar air heater with mass flow rates for different values of duct height

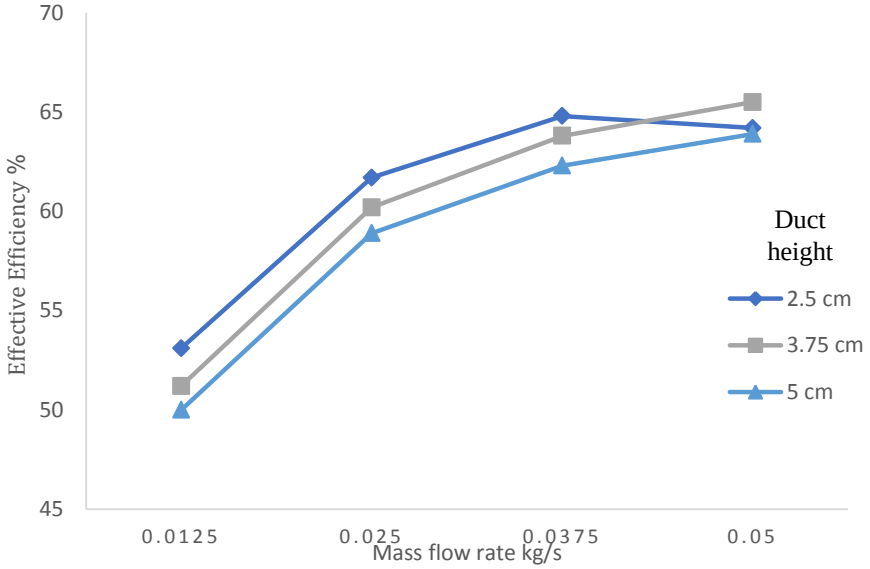

Fig. 9 Variation of effective efficiency of solar air heater with mass flow rates for different values of duct height

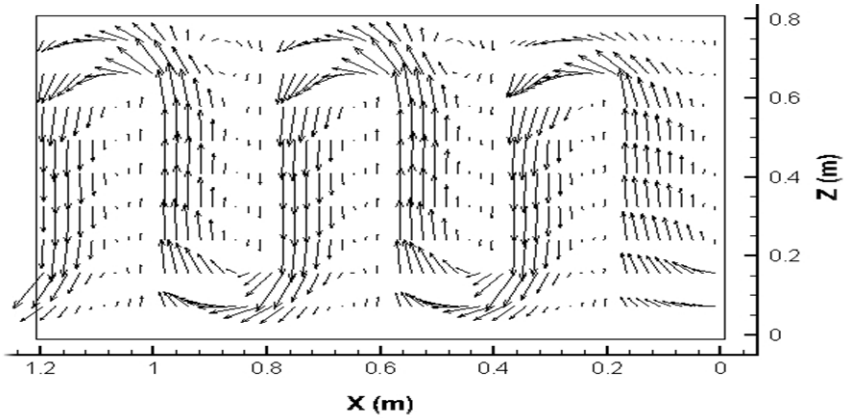

Fig. 10 Velocity vectors of airflow with mass flow rates of 0.05kg/s and duct height of 3.75 cm.

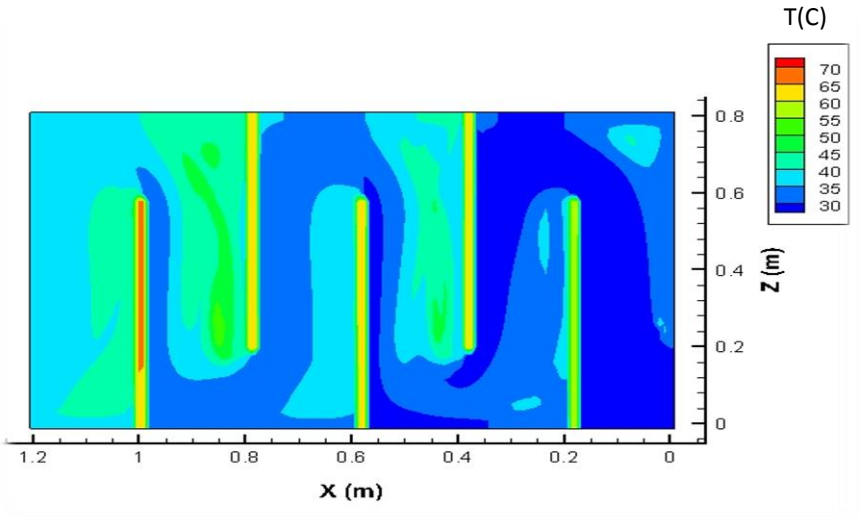

Fig. 11 Temperature contour (x z plane) at y = 2.7 cm with mass flow rate of 0.05 kg/s and duct height of 3.75 cm.

6. Conclusions and Recommendations

The following were concluded:

1. The highest value of thermal efficiency of solar air heater with straight baffles is 68.5% at duct height of 2.5 cm and mass flow rate of 0.05 kg/s.
2. The optimum value of effective efficiency of solar air heater with straight baffles is 65.5% at duct height of 3.75 cm and mass flow rate of 0.05 kg/s.

Based on this work, the following are recommended for future works:

1. Investigate the effect of adding ribs or obstacles in the passage of airflow.
2. Study the effect of baffles length and baffles pitch on the thermohydraulic performance of solar air heater.

Nomenclature

Symbols

C_μ, $C_{1\varepsilon}$, $C_{2\varepsilon}$ = Constants in turbulence model

k = Turbulent kinetic energy = $\frac{1}{2}\left(u'^2 + v'^2 + w'^2\right)$ m^2/s^2

P = Mean static pressure, N/m^2

T = Mean Temperature, °C

U, V, W = Dimensionless velocities in X, Y, Z directions, m/s

Q_u = Useful energy, W

$\dot{m}$ = Mass flow rate, kg/s

c_p = Specific heat capacity

T_o = Outlet temperature,°C

T_i = Inlet temperature, °C

η_{th} = Thermal efficiency

I = solar radiation, W/m^2

A_c = Collector area, m^2

η_{eff} = Effective efficiency

p_m = Mechanical energy consumption, W

Δp = Differential pressure, pa

Greek Symbols

ε = Dissipation rate of turbulent kinetic energy

ρ = Density of air, kg/m^3

σ_k, σ_ε = Turbulent Prandtl numbers for k, ε

ν_t = Eddy or turbulent viscosity, m^2/s

ν_e = Effective kinematics viscosity, m^2/s

Γ_e = Effective diffusion coefficient, $\Gamma = \mu_e / \sigma_e$, $N.s/m^2$

ϕ = General dependent variable

S_ϕ = Source term

References

1. E.K. Akpinar and F. Koçyiğit, "Experimental investigation of thermal performance of solar air heater having different obstacles on absorber plates," International Communications in Heat and Mass Transfer, Vol. 37, pp. 416–421, 2010.
2. R. Karwa, S.C. Solanki and J.S. Saini, "Thermo-hydraulic performance of solar air heaters having integral chamfered rib roughness on absorber plates," Energy, Vol. 26, pp.161–176, 2001.
3. K.R. Aharwal, B.K. Gandhi and J.S. Saini, "Experimental investigation on heat-transfer enhancement due to a gap in an inclined continuous rib arrangement in a rectangular duct of solar air heater," Energy, Vol. 33, pp. 585–596, 2008.

4. A.M. Lanjewar, J.L. Bhagoria and R.M. Sarviyac, "Performance analysis of W-shaped rib roughened solar air heater," Journal of Renewable and sustainable energy, Vol. 3, pp. 043110, 2011.
5. K. Pottler, C.M. Sippel, A. Beck and J. Fricke, "Optimised finned absorber geometries for solar air heating collectors," Solar Energy, Vol. 67, pp. 35-52, 1999.
6. A. Priyam and P. Chand, "Thermal and thermohydraulic performance of wavy finned absorber solar air heater,". Solar Energy, Vol. 130, pp. 250–259, 2016.
7. A.H. Falih, "Thermal Behavior in Dimple Square Duct with Inclined Perforated Baffles," Engineering and Technology Journal, Vol. 34, pp. 2047-2056, 2016
8. S. Chamoli and N. Thakur, "Performance study of solar air heater duct having absorber plate with V down perforated baffles," Songklanakarin J. Sci. Technol., Vol. 36, pp. 201-208, 2014.
9. R. Kumar, A. Kumar, R. Chauhan and M. Sethi, "Heat transfer enhancement in solar air channel with broken multiple V-type baffle," Case Studies in Thermal Engineering, Vol. 8, pp. 187–197, 2016.
10. A. Kumar and M.H. Kim, "Thermal Hydraulic Performance in a Solar Air Heater Channel with Multi V-Type Perforated Baffles," Energies, Vol. 9, pp. 564, 2016.
11. M.A. Karima and M.N.A. Hawlader, "Performance investigation of flat plate, v-corrugated and finned air collectors," Energy, Vol. 31, pp. 452–470, 2006.
12. S.V. Patanker, "Numerical heat transfer and fluid flow" McGraw-Hill, New York, 1980.
13. B.T. Launder and D.B. Spalding, "Lecturers in Mathematical models of turbulence," Department of Mechanical Engineering, imperial college of Science and Technology, London, England, 1972.
14. G. Fraisse, K. Johannes, V Berdal & G. Achard, "The use of a heavy internal wall with a ventilated air gap to store solar energy and improve summer comfort in timber frame houses," Energy and Buildings, vol. 38, pp: 293–302, 2006.
15. J.M. Jalil, K.F. Sultan, L.A. Rasheed," Numerical and Experimental Investigation of Solar Air Collectors Performance Connected in Series," Engineering and Technology Journal, Vol. 35, pp. 190-196, 2017.